Supporting Information

Infrared nano-imaging reveals the surface metallic plasmons in topological insulator

Jian Yuan[†,‖], *Weiliang Ma*[†,‖], *Lei Zhang*[‡,‖], *Yao Lu*[†], *Meng Zhao*[⊥], *Hongli Guo*[#], *Jin Zhao*[#], *Wenzhi Yu*[†], *Yupeng Zhang* [§, £], *Kai Zhang*[⊤], *Hui Ying Hoh*[§, £], *Xiaofeng Li*[¶], *Kian Ping Loh*[⊥], *Shaojuan Li*[†, *], *Cheng-Wei Qiu*[‡, *] *and Qiaoliang Bao*[†, £, *]

[†]Institute of Functional Nano & Soft Materials (FUNSOM), Jiangsu Key Laboratory for Carbon-Based Functional Materials & Devices, Soochow University, Suzhou, 215123, Jiangsu, P. R. China

[‡]Department of Electrical and Computer Engineering, National University of Singapore, 4 Engineering Drive 3, Singapore 117583, Singapore

[⊥]Department of Chemistry, National University of Singapore, 3 Science Drive 3, Singapore 117583, Singapore

[#]Hefei National Laboratory for Physical Sciences at the Microscale, Department of Physics, University of Science & Technology of China, Hefei 230026, P. R. China

[§]College of Electronic Science and Technology, Shenzhen University, Shenzhen 518060, China,

[£]Department of Materials Science and Engineering, and ARC Centre of Excellence in Future Low-Energy Electronics Technologies (FLEET), Monash University, Clayton, Victoria 3800, Australia.

[⊤]i-Lab, Suzhou Institute of Nano-Tech and Nano-Bionics, Chinese Academy of Sciences, Suzhou 215123, Jiangsu, P. R. China

[¶]College of Physics, Optoelectronics and Energy & Collaborative Innovation Center of Suzhou Nano Science and Technology, Soochow University, Suzhou 215006, Jiangsu, P. R. China

[‖] These authors contributed equally to this work.

[*] Corresponding author(s): Qiaoliang Bao (Q.B.): qlbao@suda.edu.cn, qiaoliang.bao@monash.edu; Cheng-Wei Qiu (C.Q.): chengwei.qiu@nus.edu.sg; and Shaojuan Li (S.L.): sjli@suda.edu.cn.

1. Near-field at different wavelengths

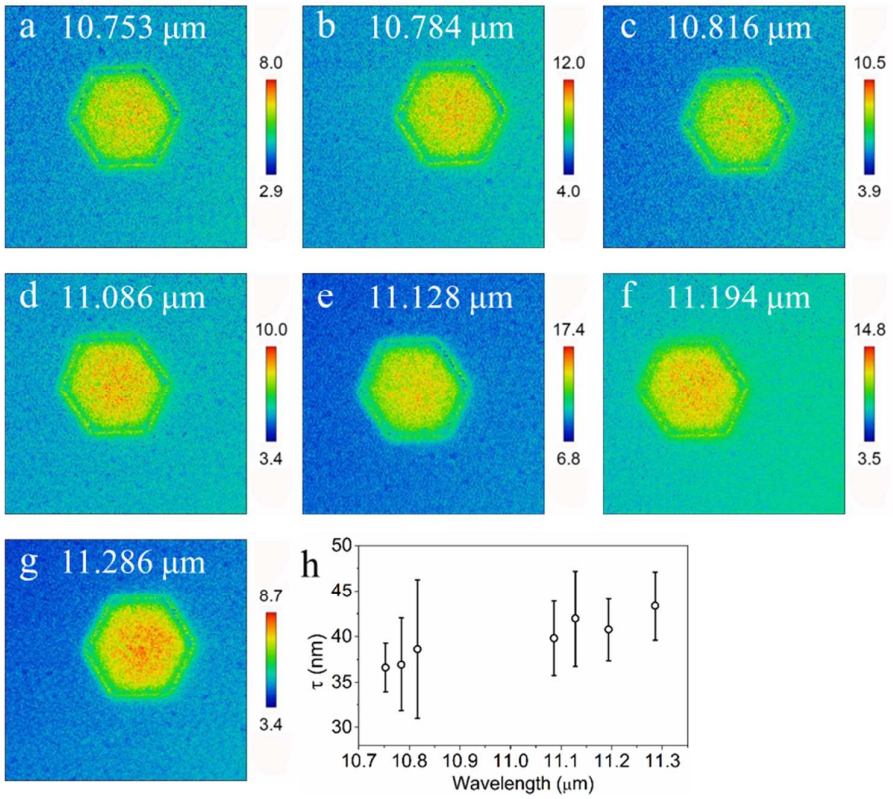

Figure S1. a-g Near-field amplitude images obtained under illumination with different wavelengths. (h) Dependence of decay length on the incident wavelength.

2. Separation of contributions from bulk and surface state to the dielectric constant of Bi_2Te_3

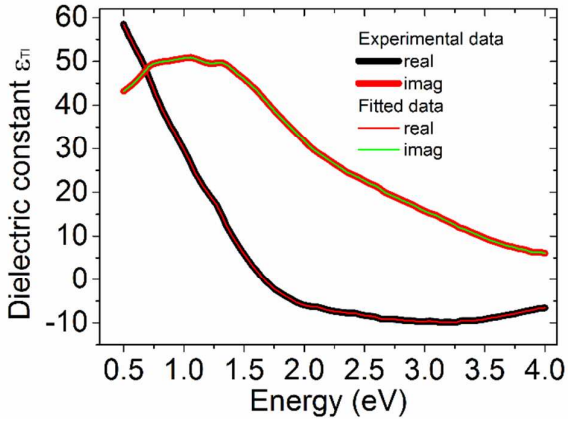

Figure S2. Comparison of experimental data and fitted data.

The complex dielectric constant can be calculated with $\varepsilon_{TI} = \varepsilon_\infty + i\sigma_{TI}/\varepsilon_0\omega$, where ε_∞ is the high-frequency dielectric constant, ε_0 is the permittivity in vacuum and σ_{TI} is the effective conductivity of topological insulators. The topologically protected surface of Bi_2Te_3 acts like a metal. Its thickness t_{surf} is assumed to be 2 nm.[1] Its conductivity could be described by Drude model. On the other hand, the inside part acts as an insulator with a thickness t_{bulk}, with conductivity described by Lorentz model. In experiment, the measured conductivity contributes from both surface and bulk parts. [1-2]

$$\sigma_{TI} = \sigma_D f_1 + \sigma_L f_2 \tag{1}$$

with $f_1 = t_{surf}/t_{total}$ and $f_2 = t_{bulk}/t_{total}$, where t_{total} is the total thickness of TI sample. The Drude part and Lorentz part can be expressed as

$$\sigma_D = \varepsilon_0 \frac{\omega_p^2}{\gamma_D - i\omega} \tag{2}$$

and

$$\sigma_L = -i\varepsilon_0\omega\left(\varepsilon_\infty - 1\right) + \frac{\varepsilon_0\omega_{pL}^2\omega}{i\left(\omega_{0L}^2 - \omega^2\right) + \omega\gamma_L}, \tag{3}$$

where ω_p and γ_D are the plasma frequency and damping rate of the Drude component, respectively. ω_{pL}, ω_{0L} and γ_L are the plasma frequency, oscillator frequency and the scattering rate of the Lorentz component, respectively. ε_∞ was set to be 1 in our fitting.

As shown in Figure S2, the dielectric constant of Bi_2Te_3 was measured from a sample with an average thickness of 12 nm. By using the equations above, we can fit the experimental data to obtain all the parameters, as shown in Table 1. Then in the following simulations, the surface layer is modeled with Drude component with a thickness of 2 nm, while the thickness of insulator part varies as that in the experiments. In order to finely simulate the surface layer, a thickness of 0.25 nm is used along the direction normal to surface.

Table 1. Fitting parameters

Fitting parameters	value
Total thickness (nm)	12
Surface thickness (nm)	2
ω_p (Drude part, eV)	4.5
γ_p (Durde part, eV)	0.7
ω_{pL} (Lorentz part, eV)	16.58
ω_{oL} (Lorentz part, eV)	1.74
γ_L (Lorentz part, eV)	3.35

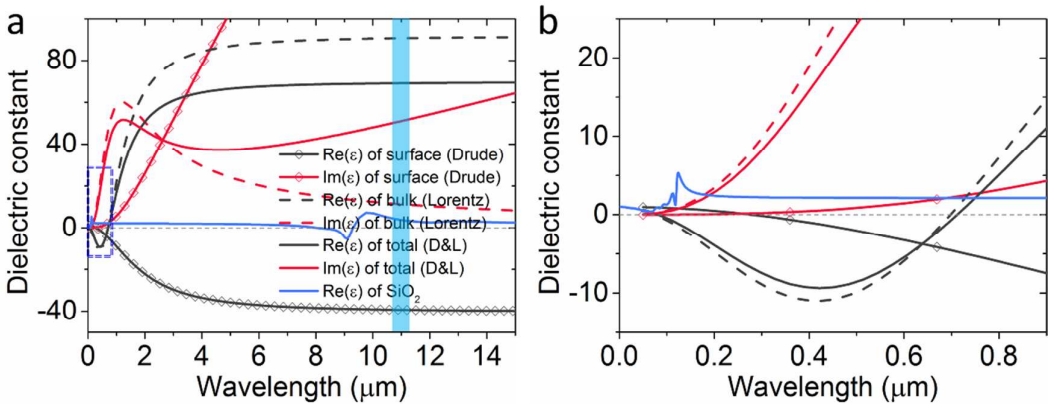

Figure S3. (a) Seperation of contributions from bulk (Lorentz) and surface (Drude) model to the total dielectric constant of Bi_2Te_3 and sampled data of SiO_2 from FDTD material database. The light blue area shows the wavelength range in our experiments. (b) Zoom-in plot of dielectric contrant at visible wavelength range, labeled by blue dashed line in (a).

As shown in Figure S3, the real part of dielectric constant of Drude contribution to Bi_2Te_3 remains negative when the wavelength is larger than 0.28 μm. Such a broad band wavelength with negative real part of dielectric constant indicates that the topologically protected surface state of Bi_2Te_3 could support surface plasmon resonance covering frequency range from ultraviolet to far infrared wave, which

shows huge difference from noble metals and even bulk state of Bi_2Te_3 itself. In constast, the real part of dielectric constant of Lorentz contribution is negative for wavelength smaller than 0.7 μm, which indicates the support of plasmonic mode at visible and ultraviolet range, as reported in our previous work.[3-4] In visible range, both surface and bulk parts could contribute to the excitation of surface plasmon resonance under certain conditions. In particlar, both parts could simulatenously support SPR in the same environment due to the same real part of dieletric constant at ~ 638 nm. However, only the surface layer can support surface plasmon resonance at long wavelength range.

3. Discussion on the near-field contrast factor

The finite-dipole model is well applied to calculate the scattered signal from the tip-sample interaction of infrared s-SNOM system. The probing tip is modeled as an isolated spheroid which is polarized by both the illuminating field and the Fresnel reflection of the resulting near-filed at the sample surface.[5] The scattered field is dependent on the near-field interaction. The s-SNOM amplitude images usually provide the material contrast rather than absolute value. Using the finite dipole-model, the near-field contrast factor η can be defined as an illumination-independent measure of the s-SNOM signal,

$$\eta = \frac{\beta\left(g - \frac{R+H}{L}\right)\ln\frac{4L}{4H+3R}}{\ln\frac{4L}{R} - \beta\left(g - \frac{3R+4H}{4L}\right)\ln\frac{2L}{2H+R}}, \tag{4}$$

with the electrostatic reflection factor

$$\beta = \frac{\varepsilon_s - 1}{\varepsilon_s + 1}. \tag{5}$$

where ε_s is the dielectric function of the detected sample, R is the radius of the spheroid on the top of the probing tip, L is the half-axial length along the major axis

of the spheroid, H is the distance between the spheroid apex and the sample surface, g the ratio of the effective point charge and the totally induced charge on a grounded spheroid, which is roughly a constant for tip-sample distance larger than $R/2$. It is thus clear that the contrast factor is mainly dependent on the materials properties when measurement is performed with a given s-SNOM system. Eq. (4) can be reformed as

$$\frac{1}{\eta} = \frac{A}{\beta} - B, \tag{6}$$

where A and B are determined by geometry parameters and g.

As shown in Figure S3, real part of total dielectric constant increases for larger wavelength, which leads to larger b, according to Eq. (5). As shown in Figure S3, the variation in the calculated dielectric constant is almost negligible at the wavelength of interest, which well explains the constant signal ratio at areas A and B in Figure 2.

REFERENCE

(1) Tang, C. S.; Xia, B.; Zou, X.; Chen, S.; Ou, H.-W.; Wang, L.; Rusydi, A.; Zhu, J.-X.; Chia, E. E., Terahertz conductivity of topological surface states in $Bi_{1.5}Sb_{0.5}Te_{1.8}Se_{1.2}$. *Sci. Rep.* **2013**, 3, 3513.

(2) Ou, J. Y.; So, J. K.; Adamo, G.; Sulaev, A.; Wang, L.; Zheludev, N. I., Ultraviolet and visible range plasmonics of a topological insulator. *Nat. Commun.* **2014,** *5,* 5139.

(3) Zhao, M.; Bosman, M.; Danesh, M.; Zeng, M.; Song, P.; Darma, Y.; Rusydi, A.; Lin, H.; Qiu, C. W.; Loh, K. P., Visible surface plasmon modes in single Bi2Te3 nanoplate. *Nano Lett.* **2015**, *15 (12),* 8331-8335.

(4) Zhao, M.; Zhang, J.; Gao, N.; Song, P.; Bosman, M.; Peng, B.; Sun, B.; Qiu, C. W.; Xu, Q. H.; Bao, Q., Actively Tunable Visible Surface Plasmons in Bi_2Te_3 and their Energy‐Harvesting Applications. *Adv. Mater.* **2016,** *28,* 3138–3144.

(5) Cvitkovic, A.; Ocelic, N.; Hillenbrand, R., Analytical model for quantitative prediction of material contrasts in scattering-type near-field optical microscopy. *Opt. Express* **2007**, *15 (14)*, 8550-8565.